Temporal Correlation Modification by Microbubbles Injection Near-Wall in a Channel Flow

by

Yassin A. Hassan[(1)], C. del C. Gutiérrez-Torres, J. A. Jiménez-Bernal, E. Domínguez-Ontiveros

Texas A&M University

Nuclear Engineering Department

College Station, Texas 77843-3133; USA

[(1)]E-Mail: y-hassan@tamu.edu

ABSTRACT

Injection of microbubbles within the boundary layer is one of the promising methods to achieve drag reduction. The environmental friendly characteristics of this method make it suitable in several applications as in large ships, pipe line transportation of fluids, etc. Although this phenomenon has been studied for several decades, the physical mechanism of drag reduction by microbubbles injection is still not clearly understood.

In an effort to achieve a better understanding of the drag reduction mechanism by microbubbles injection, the structure of flow turbulence in a water channel with microbubbles is studied using particle image velocimetry technique (PIV) at Re_h = 5128. Two-dimensional full field of the velocity components (streamwise and normal) within a location close to the wall was measured. The effects of several values of local void fraction upon the drag reduction and the time scales are investigated. To do so, the autocorrelation coefficient is calculated for both, the streamwise and normal velocity for single phase flow and two-phase flow at different void fraction values.

1. INTRODUCTION

Microbubbles injection within the boundary layer for drag reduction has been the subject of several investigations for a number of years. In 1973, McCormick and Bhattacharyya presented a pioneer work of drag reduction by microbubbles' injection using electrolysis as means of microbubbles' production. They mounted a cathode to a hull (3-foot long body of revolution with a maximum diameter of 5 inch) and then created hydrogen bubbles beneath the boundary-layer by passing a current through the cathode. The hull was mounted to a force dynamometer which allowed measuring the drag force and towed along a tank at a constant mean depth. It was found that the amount of drag reduction depends on the towing speed and the time-rate of hydrogen production.

Bogdevich, et al. (1977), performed experiments of saturation of bubbles in the turbulent boundary layer of a flat plate and in the initial section of a channel. Their results showed a dependency on the value of the Reynolds number and the local friction. After increasing the Reynolds number above its critical values, it was observed that the efficiency of the gas saturation in reducing the drag is increased. Results presented by Merkle and Deutsh (1989) showed that the effect of the bubbles on the boundary layer had a strong dependence upon both their concentration and their location in the boundary layer. Microbubbles were more effective in the buffer layer. It was also observed that the diameter of the bubbles played a significant role in the drag reduction phenomenon.

Skin friction measurements were carried out by Guin, et al. (1996). It was confirmed that the microbubble drag reduction is inner-region dependent. In contrast with other drag reduction methods there seems to be an absence of outer-layer influence in this phenomenon. This was can be inferred from the lack of influence of the bubble distribution patterns away from the wall.

One of the early numerical simulations in drag reduction by microbubble injection was performed by Madavan et al. (1985). They used a simple mixing-length eddy-viscosity formulation, whose functional form is unchanged by the presence of bubbles. The effect of the bubbles on the boundary-layer characteristics are taken into account by allowing the viscosity and density to vary locally as a function of a prescribed bubble concentration profile. The results obtained indicated that the magnitude of skin-friction reduction depends upon the volumetric concentration of the bubbles, and also on their location and distribution within the boundary layer. The presence of bubbles in the viscous layer and the absence of bubbles in the buffer layer appeared to make the bubbles less effective.
The marker-density-function (MDF) method was developed by Kanai and Miyata (2001) to conduct direct numerical simulation (DNS) for bubbly flows. The method was applied to a turbulent bubbly channel flow to elucidate the interaction between bubbles and wall turbulence. It was found out that the interaction between the bubbles and the wall turbulence near the wall contributes to the reduction of turbulent energy. The necessity of concentration of the bubbles near the wall, specifically within the buffer layer, to attain drag reduction was pointed out.

A series of numerical simulations of small bubbles seeded in a turbulent channel flow at average void fractions of up to 8% were carried out by Xu et al. (2002). They carried out a DNS simulation using the force-coupling method (FCM) to simulate the presence of the bubbles and their influence on the flow. The effects of bubble seeding levels, bubble size and interactions with the turbulent flow were computed. Turbulence modification was observed in the presence of microbubbles in the form of lifted streaks, which become more coherent while the spaces of the streaks increased for the cases where drag reduction was obtained.

The turbulence structure of flow field including microbubbles in a horizontal channel was experimentally investigated by Kitagawa, et al. (2003) using particle tracking velocimetry and Laser Induced Fluorescence (PTV/LIF) technique. It was clarified from the obtained results that the turbulence intensity increases while the Reynolds stresses decrease with increasing void fraction.

2. EXPERIMENTAL METHOD and PROCEDURES

2.1 Experimental Set-up

The experiment was carried in a rectangular cast acrylic channel with 4.8 m length, 20.5 cm wide and 5.8 cm height. The two-dimensional velocity full field, at a location about 3.15 m downstream (L/D_h=35), is measured by particle image velocimetry (PIV) technique.

The illumination source for the PIV system is a high power, dual oscillator Nd:YAG laser. The energy per pulse is about 350 mJ. The particle seeds used for tracing the flow have micron diameters range from 6-9 μm with specific gravity of 1.01 close to water's specific gravity.

The scattered laser light from the seeding particles was recorded using a CCD Kodak Megaplus camera, Model Megaplus ES 1.0/10, with an array of 1008 x 1018 pixels. The viewing area was 1.28 cm^2 and was located close to the upper channel wall. The system recorded 30 velocity fields per second. Each velocity field was obtained from a pair of consecutive images capturing the second image of the pair after a duration of 1ms after of the previous image via frame straddling approach. Images were recorded for a time span of approximately 3.3 sec.

The pressure gradient in the test section was measured with pressure taps positioned on the top wall of the channel over a length of 157.5 cm. A Validyne pressure transducer (Model DP103) was used. This transducer has a range of pressure difference of 0-35 Pascal. To estimate the wall shear stress from the pressure drop measurements of fully developed single phase channel flow, the following equation is used:

$$\tau_w = -h\frac{\Delta P}{\Delta x} \tag{1}$$

where, t_w is the wall shear stress, ΔP, is the pressure drop measured by the pressure transducer, Δx, is the axial distance between the pressure connection tabs and h is the half height of the channel. The value of the wall shear stress for single phase flow was compared with the wall shear stress inferred from the PIV velocity components measurements.

Hydrogen microbubbles are produced by electrolysis at 10 cm upstream the test zone. Platinum wires with diameter of 76 μm is used as electrodes. To produce hydrogen microbubbles of 30 μm, a current of 25 mA is conducted through the electrodes. The negative electrode (cathode) produces hydrogen microbubbles whereas the positive one (anode) produces oxygen microbubbles. A schematic of the channel set up is illustrated in figure 1.

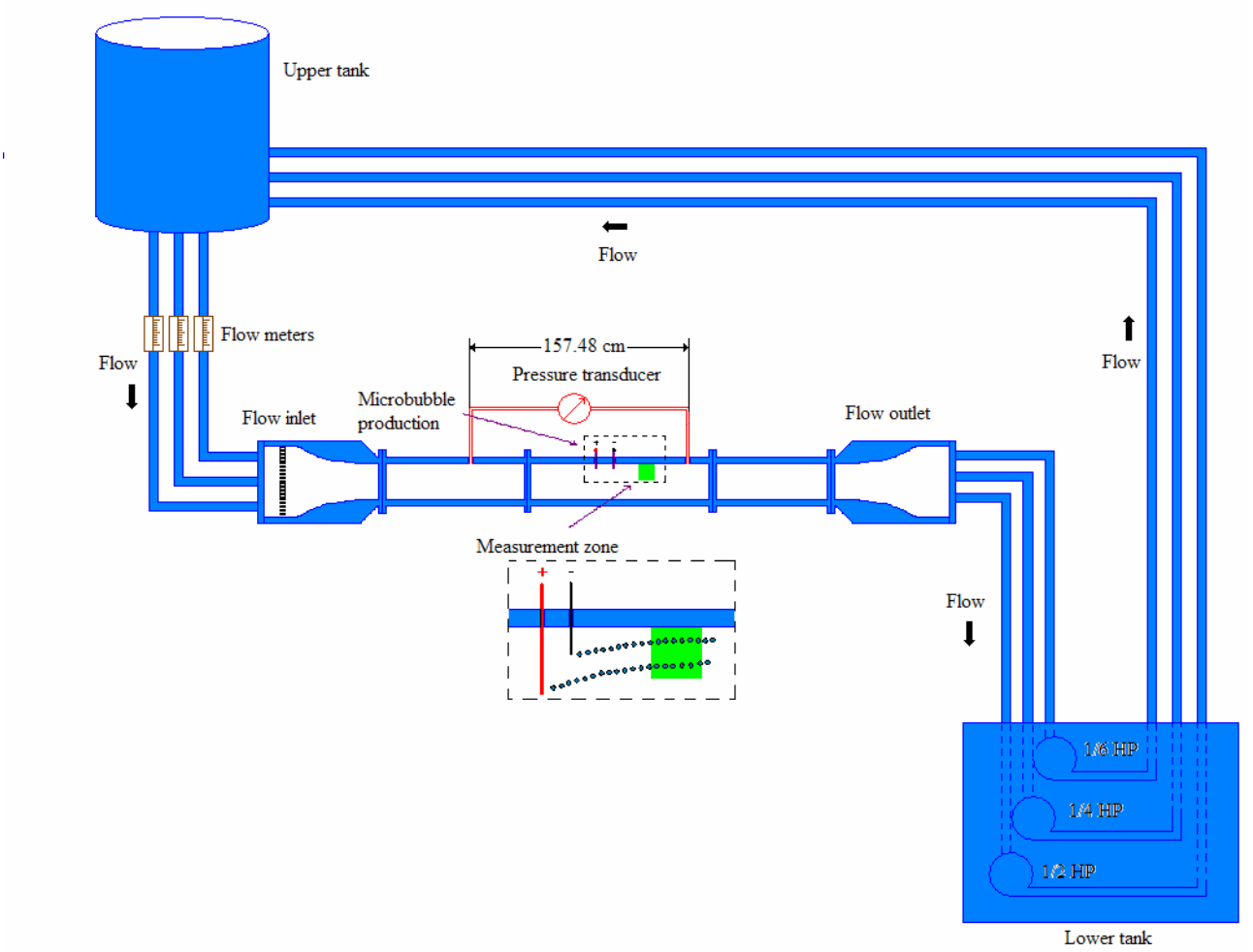

Fig. 1. Schematic drawing of experimental set up.

2.2 PIV procedure

In this study, the particle tracking is performed through a cross correlation algorithm. Two different software applications were used for the tracking process. The resulting velocity vectors from each application were then compared, corrected and combined.

The first application works in a windows environment. One of its advantages is flexibility about the number of images that can be processed at the same time making possible to process just one pair of images or the whole set of images at once. This characteristic facilitates the setting of the image threshold and tracking conditions. This software is based on successive abandonment (SA) method. This method (SA) was modified using selected characteristic pixels which have the highest intensity and the lowest one in a line of an interrogation window. By this method, difference between correct candidate and other ones becomes clear and the SA method can be accelerated. Combined by this selected pixel approach and error detection suitable for SA, high-speed super-resolution PIV is achieved (Yamamoto et al., 2002).

The other tracking process is an in-house routine (Hassan et al. 1992), which it has been improved over the last fifteen years. This application is not windows environment friendly, and it runs on a UNIX environment. It requires the binarization of the images. The image processing and conversion are performed through a developed application with the LabView programming environment. The tracer particle centroid algorithm runs in UNIX enviroment. This tracking method can be performed between two sequential, high resolution images. The particle velocity is calculated by determining the correspondence between particles in two sequential frames. The correspondence is obtained through calculation of a correlation coefficient between a referenced pattern in the first binary image and a possible candidate

pattern in the second binary image, where the latter is shifted so that the centroids of the possible particle pair coincide. The velocity for a particle is determined by the particle displacement divided by the image acquisition time.

Prior to the velocity field interpolation, a filter process was used to remove incorrect velocity vectors. The interpolation of the velocity field was obtained by an inverse distance algorithm (AMTEC, 1998) using a window of 20x20 pixels. The final results are instantaneous velocity fields where the vectors are distributed in an ordered grid of 50x50 vectors.

Detection of microbubbles in the two-phase flow was carried out using similar software applications for liquid phase flow applying thresholds to the size of the bubbles detected by the programs and to the brightness of the bubbles. Since microbubbles are larger and brighter than the seed particles, they can be easily distinguished from the seeds.

3. RESULTS AND DISCUSSION

For statistically stationary processes, the simplest multi-time statistic that can be considered is the autocorrelation coefficient (Pope, 2000), also known as the Lagrangian correlation, which can be expressed as

$$R_{ij}(\Delta t) = \frac{\overline{u'_i(t)u'_j(t+\Delta t)}}{u_{rms_i}(t)u_{rms_j}(t+\Delta t)} \tag{2}$$

where u'_i is the fluctuating velocity component at the time t, and Δt is the delay time.

The autocorrelation function has the properties

$$R_{ij}(0) = 1 \tag{3}$$

$$\left|R_{ij}(\Delta t)\right| \le 1 \tag{4}$$

For processes present in turbulent flows, the correlation diminishes as the lag time Δt increases.

To calculate the temporal correlation coefficients at a specific location within the measurement zone, the fluctuating velocity, obtained from PIV measurement, was followed in time. The recording time span of the measurements was about 3.3sec. This is equivalent to 200 images. The autocorrelation coefficients for u' and v' fluctuating velocities which were calculated at a location $x^+ = 69.7$ and $y^+ = 17.4$ are presented in figures 2 and 3, respectively for single phase flow and values of local void fraction, α = 4.4 and 4.9%; where the void fraction within the viewing area is defined as $\alpha = \frac{V_g}{V_l + V_g}$, V_g = volume of gas within the viewing area and V_l = volume of liquid.

One effect of the microbubbles presence within the boundary layer is a decrease in the drag. The drag reduction, DR, is calculated by $DR = 1 - \frac{\tau_{w,\text{water and bubbles}}}{\tau_{w,\text{water}}}$. The drag reduction, DR, cab also be expressed as $DR = 1 - \left(\frac{u_{\tau_{\text{microbubbles}}}}{u_{\tau_{\text{water}}}}\right)^2$; where $u_{\tau_{\text{water}}}$ and $u_{\tau_{\text{microbubbles}}}$ are the friction velocity without microbubbles and with microbubbles, respectively. The drag reduction of value of 29.8% and 38% are achieved with void fractions of 4.4% and 4.9%.

Another effect of the microbubbles' presence within the boundary layer is an increase in the autocorrelation values for the streamwise fluctuating velocity component. However, the opposite effect is observed for the normal velocity components.

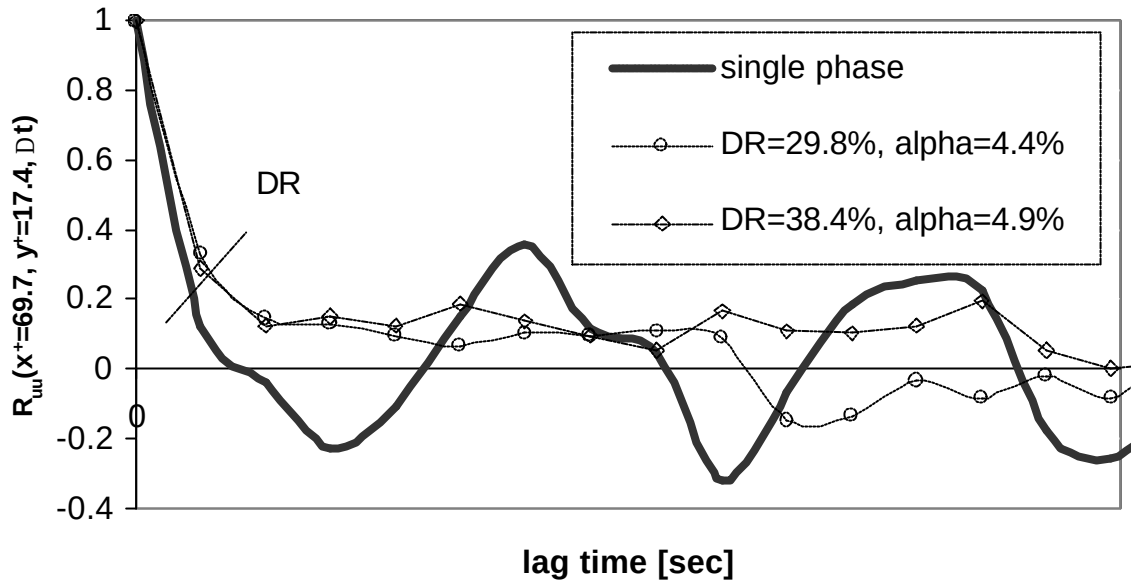

Fig. 2. Temporal autocorrelation coefficients for streamwise velocity u' at $x^+ = 69.7$ and $y+=17.4$.

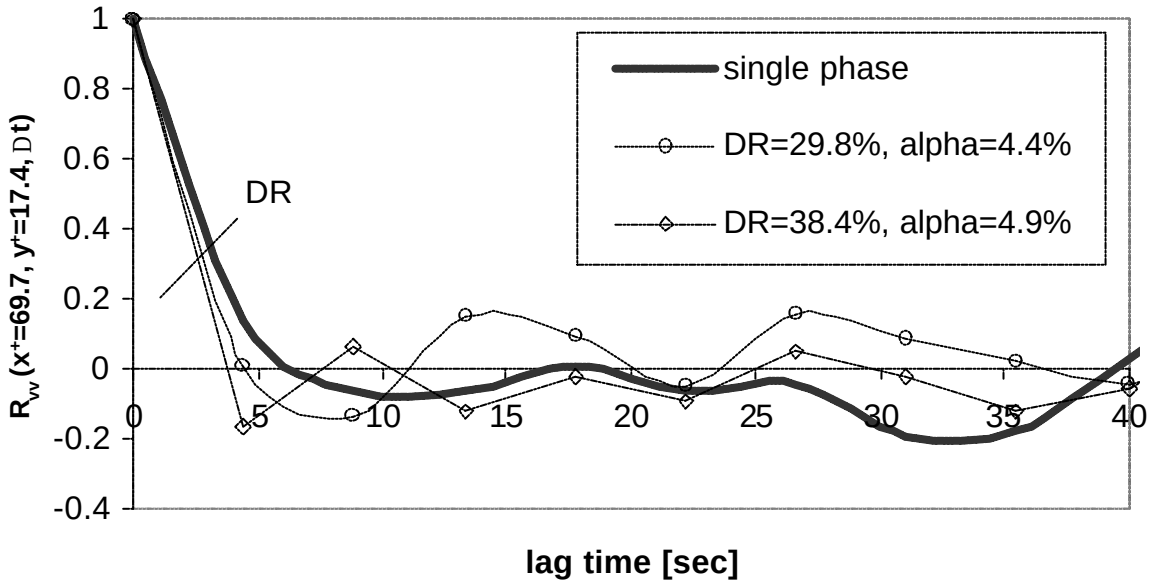

Fig. 3. Temporal autocorrelation coefficients for normal velocity v' at $x^+ = 69.7$ and $y+=17.4$.

This behaviour is also observed at a different position, farther from the wall. A persistent increase in the autocorrelation coefficient is observed for the streamwise velocity fluctuation at $x^+ = 69.7$ and $y^+ = 28.4$. Again, the opposite trend is observed for the autocorrelation calculated using the normal velocity fluctuation. This is presented in figures 4 and 5.

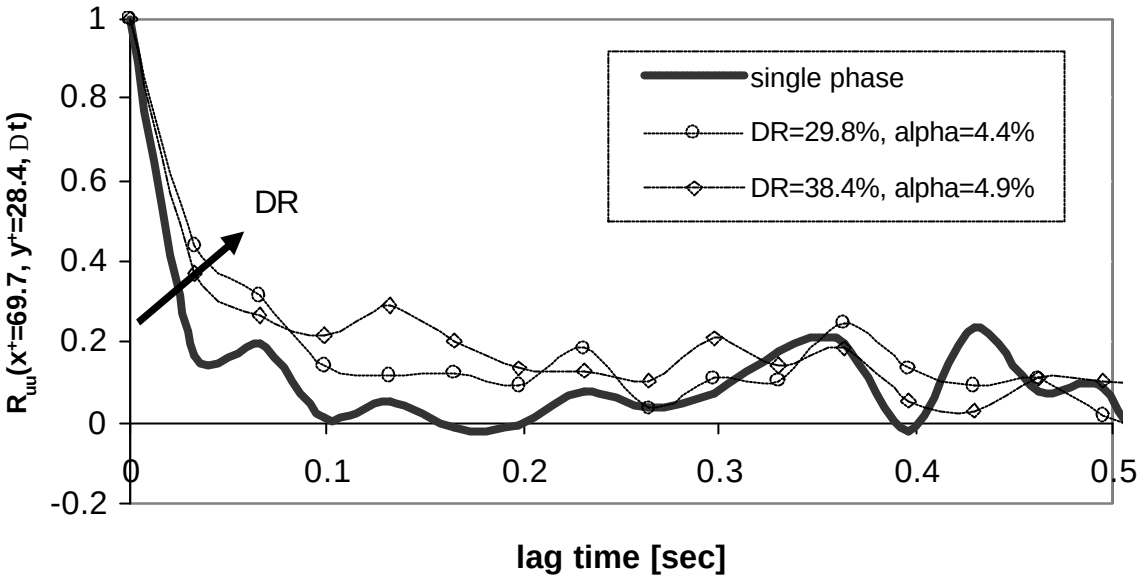

Fig. 4. Temporal autocorrelation coefficients for streamwise velocity u' at $x^+ = 69.7$ and $y+=28.4$.

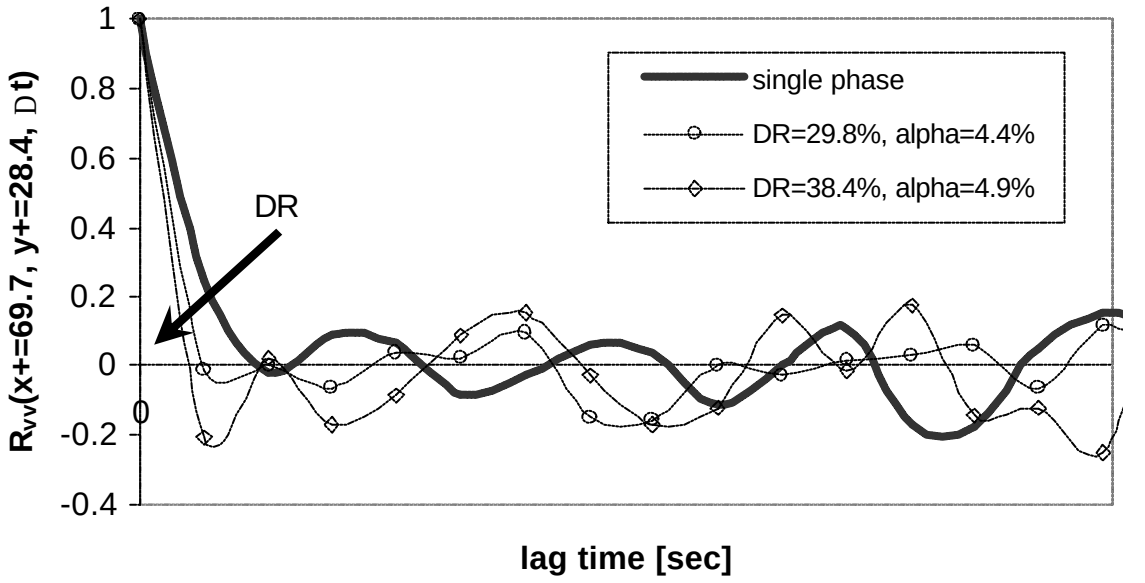

Fig. 5. Temporal autocorrelation coefficients for normal velocity v' at $x^+ = 69.7$ and $y+=28.4$.

The integral time scales vary with position in the flow unless it is homogeneous as well as steady. One can define integral correlation times as:

$$T_L = \int_0^b R_{ij}(\Delta t)dt \tag{5}$$

where T_L is the integral time scale, $R_{uu}(t)$ is the autocorrelation function and, b, is the first time value at which the autocorrelation curves crosses the x-axis. Tables 1 and 2 show the values of the integral time scale for u' and v' fluctuating velocities calculated from the autocorrelation values at ($x^+ = 69.7$, $y^+ = 17.40$) and ($x^+ = 69.7$, $y^+ = 28.4$) respectively.

Table 1. Integral time scales from autocorrelation coefficients at $x^+ = 69.7$, $y+ = 17.4$

($x^+ = 69.7$, y+ = 17.4)	Single phase	DR=29.8%, α=4.4%	DR=38.4%, α=4.9%
T_{Lu} [ms]	12	47	72
T_{Lv} [ms]	11	7	5

Table 2. Integral time scales from autocorrelation coefficients at $x^+ = 69.7$, $y+ = 28.4$

($x^+ = 69.7$, y+ = 28.4)	Single phase	DR=29.8%, α=4.4%	DR=38.4%, α=4.9%
T_{Lu} [ms]	20	80	100
T_{Lv} [ms]	15	8	4

The time scale of the streamwise velocity components is increased, while the time scale of normal velocity components is decreased. This indicates that the transport of flow information in the streamwise velocity is enhanced; while in the normal direction is reduced.

4. SUMMARY

Particle Image Velocimetry is used to measure the velocity field in an x – y plane close to the upper wall in a channel. The evaluation of the autocorrelation coefficient values at different location within the measurement area shows changes in the integral time scale for the streamwise and normal fluctuating velocities. This changes in the integral time scale values (increase for u' and decrease for v') suggest that the transport of flow information in the streamwise velocity is enhanced; while in the normal direction is reduced.

REFERENCES

AMTEC Engineering. (1998). "Tecplot version 8.0 User's manual", Bellevue, Washington.

Bogdevich, V. G., Evseev, A. R., Malyuga, A. G. and Migirenko, G. S. (1977) "Gas-saturation effect on near-wall turbulence characteristics" In Drag Reduction, papers presented at the second international conference on drag reduction, pp.D2-25 – D2-37.

Guin, M. M., Kato, H., Yamaguchi, H., Maeda, M. and Miyanaga, M. (1996) "Reduction of skin friction by microbubbles and its relation with near-wall bubble concentration in a channel", J. Mar. Sci. Technol., 1, pp. 241-254.

Hassan, Y. A., Blanchat, T. K. and Seeley, C. H. Jr. (1992) "PIV flow visualization using particle tracking techniques", Meas. Sci. Technol., 3, pp. 633-642.

Kanai, A. and Miyata, H. (2001) "Direct numerical simulation of wall turbulent flows with microbubbles", Int. J. Numer. Meth Fluids, 35, pp. 593-615.

Kitagawa, A., Sugiyama, K., Ashihara, M., Hishida, K. and Kodama, Y. (2003) "Measurement of turbulence modification by microbubbles causing frictional drag reduction". In: Proc. of ASME FEDSM'03.

Madavan, N. K., Merkle, C.L. and Deutsch, S. (1985) "Numerical investigations into the mechanisms of microbubble drag reduction", Journal of Fluids Engineering. Transactions of ASME, 107, pp. 370-377.

McCormick, M. E. and BHATTACHARYYA, R. (1973) “Drag reduction of a submersible hull by electrolysis”, Naval Engineers Journal April,, pp. 11-16.

Merkle, C. L. and Deutsch, S. (1989) “Microbubble drag reduction”, Frontiers in Experimental Fluid Mechanics Ced. M. Lecture Notes in Engineering, 46, pp. 291-335.

Pope, S. B. (2000) “Turbulent Flows”, Cambridge University Press.
Xu, J., Maxey, M. R. and Karniadakis, G. E. (2002) “Numerical simulation of turbulent drag reduction using micro-bubbles”, J. Fluid Mech., 468, pp. 271-281.

Yamamoto, Y., Uemura, T. and Kadota, S. (2002) “Accelerated super-resolution PIV based on successive abandonment method”, In: Proceedings of 11th International Symposium on Applications of Laser Techniques to Fluid Mechanics.